decreasing σ-donor and increasing π-acceptor strengths of the trans L group.[2] Although some pK_a values are too close (those for 4-pic and py and those for isn, 4-acpy, and pz) to be used to make a very definite distinction in the σ and π acidity of the trans ligands, the approximate ligand acidity order is NH_3 < 4-pic $\lesssim$ py < isn $\lesssim$ 4-acpy $\simeq$ pz < pzH^+ in these complexes.

Reduction Potentials. Formal reduction potentials of *trans*-$Ru(NH_3)_4(L)L'^{3+/2+}$ determined by cyclic voltammetry are listed in Table IV. The CV values of each complex fitted most of the criteria for a reversible couple.[12] A CV of the reversible $Ru(NH_3)_5py^{3+/2+}$ couple was run under the same conditions and its values were used for comparison. Peak to peak separations increased (from 57 to 72 mV) with increasing scan rate (in different ranges, from 10 to 500 mV), which might be due to cell resistance. Some differences in the values of formal reduction potentials appeared in the literature (Table IV), and in some cases the differences are attributed to different experimental conditions.[3,13]

Previous observations showed that π-unsaturated ligands, such as pyridines (py-X), lead to substantially more positive reduction potentials for the $Ru(NH_3)_5^{3+/2+}$ couples than when L is H_2O or NH_3 and that electron-withdrawing substituents (X) increase E_f; that is, the π-accepting abilities of the ligands increase E_f values.[14] It was also observed[13] that the substitution of a second ammonia by another ligand to give a $Ru(NH_3)_4L_2^{3+/2+}$ complex yields more positive E_f values than for the corresponding $Ru(NH_3)_5L^{3+/2+}$ complex. Again, when an ammonia of $Ru(NH_3)_5(L)^{3+/2+}$ is substituted by another ligand L' to yield $Ru(NH_3)_4(L')(L)^{3+/2+}$, more positive E_f values are also obtained. This is expected since another π-acceptor ligand, with weaker σ-donor strength, is being added, favoring the stabilization of Ru(II) relative to Ru(III). For each series of *trans*-$Ru(NH_3)_4LL'^{3+/2+}$, considering a fixed L ligand, the more positive E_f values are in general, obtained with ligands L' of higher π-acceptor and lower σ-donor abilities, and this order is the same as that observed in $Ru(NH_3)_5L'^{3+/2+}$,[14] i.e., pz > 4-acpy > isn > py > 4-pic. For *trans*-$Ru(NH_3)_4(py)L'^{3+/2+}$ and *trans*-$Ru(NH_3)_4(4\text{-acpy})L'^{3+/2+}$, the E_f values, when L' is 4-acpy or isn, are too close and could also be considered within the experimental error. However, the remaining values are sufficiently distinct to allow that ordering. The difference between E_f values of *cis*-$Ru(NH_3)_4(isn)L^{3+/2+}$ and $Ru(NH_3)_5L^{3+/2+}$, for each L, is almost the same,[3] which suggested that the two unsaturated ligands interact with a different d_π metal orbital each, and thus, the two ligands are unlikely to be coplanar in the cis isomers.[3] Similar patterns for the E_f values of *trans*-$Ru(NH_3)_4LL'^{3+/2+}$ and $Ru(NH_3)_5L'^{3+/2+}$ were not obtained. Furthermore, considering the E_f values of the *cis*- and *trans*-$Ru(NH_3)_4(isn)L^{3+/2+}$ couples, it can be observed that the cis isomers have higher values (although close) than the trans analogues. This would suggest heterocycle ligand coplanarity in the trans isonicotinamide complexes, implying that only one d_π metal orbital is involved in bonding with the heterocyclic ligands, a feature consistent with the spectral data.

Acknowledgment. This work was supported in part by grants from the CNPq (No. 40.5617/82 and 40.7302/83) and the Fapesp (No. 81/1120-7 and 83/0934-6). E.T. acknowledges a research fellowship from the CNPq (No. 30.0142-80), and M.L.B. acknowledges Master's fellowships from the Fapesp (No. 81/1381-5) and Capes. We thank Drs. D. W. Franco and G. Chiericato, Jr., for help and for allowing the use of their CV apparatus, Dr. Peter C. Ford for helpful suggestions and revision of the manuscript, and the Laboratory of Microanalysis of the Instituto de Química of the University of São Paulo.

(12) (a) Nicholson, R. S.; Shain, I. *Anal. Chem.* **1964**, *36*, 706. (b) *Ibid.* **1965**, *37*, 178.
(13) Lim, H. S.; Barclay, D. J.; Anson, F. C. *Inorg. Chem.* **1972**, 11, 1460.
(14) Matsubara, T.; Ford. P. C. *Inorg. Chem.* **1976**, *15*, 1107.
(15) Meyer, T. J., Taube, H. *Inorg. Chem.* **1968**, *7*, 2369.

Contribution from the Department of Chemistry and Laboratory for Molecular Structure and Bonding, Texas A&M University, College Station, Texas 77843

Discrete Trinuclear Complexes of Niobium and Tantalum Related to the Local Structure in Nb_3Cl_8

F. Albert Cotton,* Michael P. Diebold, Xuejun Feng, and Wieslaw J. Roth

Received June 3, 1988

The preparations of three discrete trinuclear cluster compounds of group V metals are described: $Nb_3Cl_7(PMe_2Ph)_6$, $(PEt_3H)[Nb_3Cl_{10}(PEt_3)_3]$, and $(PEt_3H)[Ta_3Cl_{10}(PEt_3)_3]$. The structures have been established in detail by X-ray crystallography and in each case there is an $M_3(\mu_3\text{-}Cl)(\mu_2\text{-}Cl)_3$ core surrounded by the remaining nine ligands. The relationship of this core structure to the subunit in Nb_3Cl_8 is discussed. The M-M distances (Å) in these three compounds are 2.832 (4), 2.976 (6), and 2.932 (3), respectively. The large difference between the first two has been correlated with the difference in the number of electrons available for Nb-Nb bonding, namely eight and six, by means of Fenske-Hall molecular orbital calculations. It is shown that in both cases there are six strongly bonding electrons and that the additional two electrons in the eight-electron case occupy another singly degenerate orbital of bonding character. The crystallographic data for the three compounds are as follows. $Nb_3Cl_7(PMe_2Ph)_6$: $P2_1/n$, a = 12.339 (2) Å, b = 27.275 (8) Å, c = 19.187 (9) Å, β = 92.76 (2)°, Z = 4. $(PEt_3H)[Nb_3Cl_{10}(PEt_3)_3]$: $P2_1/n$, a = 12.615 (1) Å, b = 18.731 (3) Å, c = 23.662 (4) Å, β = 98.59 (1)°, Z = 4. $(PEt_3H)[Ta_3Cl_{10}(PEt_3)_3]$: $P2_1/n$, a = 11.864 (3) Å, b = 20.664 (2) Å, c = 18.779 (2) Å, β = 97.61°, Z = 4.

Introduction

Infinite chains, infinite sheets, or three-dimensional arrays, which are the distinctive features of the solid state of matter, are sometimes resolvable into well-defined subunits linked by bridging atoms that are shared between them. The character of a subunit naturally plays a predominant role in determining the character of the material in which it inheres, although the strong linking together of the subunits means that the whole is not simply the sum of its parts. In attempting to understand the properties and behavior of the entire solid, it is essential to understand the subunit, and this task is, in turn, facilitated by having access to individual subunits in molecular form. To accomplish this it is necessary to make provision for satisfying the coordination requirements of the subunit by ligands that are independent of, and different from, those present in the solid state. If this can be done in a conservative way, the molecular species should be good models, although not actually replicas, of the subunits in the solid.

This report describes a successful exercise of the type just described. It may be observed first of all that there are in principle

0020-1669/88/1327-3413$01.50/0

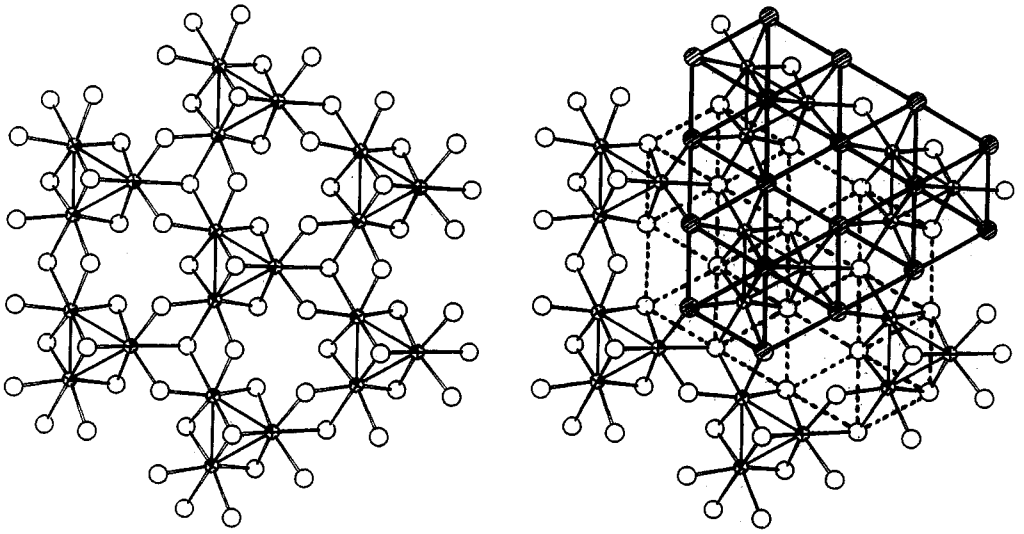

Figure 1. Portion of the infinite array of atoms in Nb_3Cl_8: left, the structure itself; right, structure with lines emphasizing the two adjacent close-packed layers.

Table I. Crystallographic Data

	$Nb_3Cl_7(PMe_2Ph)_6 \cdot C_7H_8$	$HPEt_3[Nb_3Cl_{10}(PEt_3)_3] \cdot 1.25C_7H_8$	$HPEt_3[Ta_3Cl_{10}(PEt_3)_3]$
formula	$Nb_3Cl_7P_6C_{55}H_{74}$	$Nb_3Cl_{10}P_4C_{24}H_{61} \cdot 1.25C_7H_8$	$Ta_3Cl_{10}P_4C_{24}H_{61}$
fw	1447.90	1222.01	1371.02
space group	$P2_1/n$	$P2_1/n$	$P2_1/n$
syst abs		$0k0$, $k \neq 2n$; $h0l$, $h + l \neq 2n$	
a, Å	12.339 (2)	12.615 (1)	11.864 (3)
b, Å	27.275 (8)	18.731 (3)	20.664 (2)
c, Å	19.187 (9)	23.662 (4)	18.779 (2)
α, deg	90.0	90.0	90.0
β, deg	92.76 (2)	98.59 (1)	97.61 (2)
γ, deg	90.0	90.0	90.0
V, Å^3	6650 (6)	5528 (2)	4563 (2)
Z	4	4	4
d_{calcd}, g/cm	1.491	1.468	1.995
cryst size, mm	0.35 × 0.45 × 0.45	0.25 × 0.3 × 0.5	0.3 × 0.3 × 0.4
μ(Mo Kα), cm^{-1}	9.743	12.096	78.423
data collcn instrument	CAD-4	CAD-4	CAD-4
radiation (monochromated in incident beam)	Mo Kα (λ_α = 0.710 73 Å)		Mo Kα (λ_α = 0.710 73 Å)
orientation reflcns: no.; range (2θ), deg	25, 20.0–28.0	25, 13.8–29.5	25, 15.4–31.4
temp, °C	22	22	22
scan method	ω	ω–2θ	ω
data collcn range (2θ), deg	4–45	4–50	4–50
no. unique data; tot. with $F_o^2 > 3\sigma(F_o^2)^2$	6256; 4805	6951; 5505	5501; 4047
number of params refined	605	399	325
R^a	0.054	0.047	0.039
$R_w{}^b$	0.070	0.067	0.048
quality-of-fit indicator^c	1.713	1.683	1.215
largest shift/esd, final cycle	0.64	0.23	0.61
largest peak, e/Å	0.874	0.99	1.233

$^a R = \sum||F_o| - |F_c||/\sum|F_o|$. $^b R_w = [\sum w(|F_o| - |F_c|)^2/\sum w|F_o|^2)^{1/2}$; $w = 1/\sigma^2(|F_o|)$. ^{c}Quality-of-fit $= [\sum w(|F_o| - |F_c|)^2/(N_{observns} - N_{params})]^{1/2}$.

two ways in which the molecular subunits might be obtained. The more obvious would be by treatment of the solid-state compound with a reagent that could pry the subunits apart. As we shall explain later, this method may be as bootless as it is obvious if the solid-state compound has great stability, either thermodynamic or kinetic. The other approach is to build the subunit up from scratch under conditions that trap the subunit before condensation to any extended array can occur. That is the approach we shall describe.

The compound Nb_3Cl_8 was reported more than a quarter of a century ago.[1] Figure 1 shows the structure in a way that has not previously been published. The view is in a direction perpendicular to the close-packed sheets of Cl atoms, whose nature is emphasized by the amended picture on the right. An ordered subset of the octahedral interstices between these sheets is occupied by niobium atoms so that local equilateral triangular groups are formed. Actually, the niobium atoms distort the octahedra they occupy so that they can draw together and form Nb–Nb bonds (Nb–Nb = 2.81 Å). Each of these clusters has a capping (μ_3) Cl atom above its center and three μ_2-Cl atoms beneath it that belong exclusively to it. Each cluster is then surrounded by nine more Cl atoms, three of which bridge to two other clusters and six of which bridge to one other cluster. Thus, the formula of Nb_3Cl_8 can be written in the notation introduced some years ago by H. Schäfer and others as $Nb_3Cl_4Cl_{3/3}Cl_{6/2}$.

The local cluster unit, then, is of the monocapped, edge-bridged, M_3X_{13} type, first recognized in some mixed-metal oxides of molybdenum and since extensively studied in the discrete forms Mo_3O_4, Mo_3O_3S, $M_3O_2S_2$, M_3OS_3, and M_3S_4, as well as some others.[2] Since the molybdenum clusters can be obtained in both

(1) (a) von Schnering, H. G.; Wohrle, H.; Schafer, H. *Naturwissenschaften* **1961**, *48*, 159. (b) Simon, A.; v. Schnering, H. G. *J. Less-Common Met.* **1966**, *11*, 31.

(2) For an overview and literature references see: Cotton, F. A.; Wilkinson, G. *Advanced Inorganic Chemistry*, 5th ed.; Wiley-Interscience: New York, 1988; pp 825–827, 831–835.

Table II. Positional and Equivalent Isotropic Displacement Parameters for $Nb_3Cl_7(PMe_2Ph)_6 \cdot C_7H_8$

atom	x	y	z	B,[a] Å²
Nb(1)	0.75919 (8)	0.08579 (4)	0.78369 (5)	2.87 (2)
Nb(2)	0.72423 (8)	0.15846 (4)	0.68017 (5)	2.80 (2)
Nb(3)	0.73373 (8)	0.18496 (4)	0.82324 (5)	2.84 (2)
Cl(1)	0.5910 (2)	0.1336 (1)	0.7658 (1)	3.10 (6)
Cl(2)	0.8834 (2)	0.1030 (1)	0.6854 (1)	3.76 (6)
Cl(3)	0.8463 (2)	0.2233 (1)	0.7354 (1)	3.84 (6)
Cl(4)	0.8944 (2)	0.1310 (1)	0.8586 (2)	3.91 (7)
Cl(10)	0.6631 (3)	0.0132 (1)	0.7310 (2)	4.50 (7)
Cl(20)	0.5896 (3)	0.2167 (1)	0.6270 (2)	4.90 (8)
Cl(30)	0.6441 (3)	0.1787 (1)	0.9354 (2)	4.90 (8)
P(1)	0.6589 (3)	0.0532 (1)	0.8963 (2)	4.44 (8)
P(2)	0.9162 (3)	0.0156 (1)	0.7937 (2)	3.93 (7)
P(3)	0.6106 (3)	0.0968 (1)	0.5949 (2)	3.95 (7)
P(4)	0.8427 (3)	0.1933 (1)	0.5734 (2)	3.69 (7)
P(5)	0.5784 (3)	0.2542 (1)	0.8063 (2)	4.14 (7)
P(6)	0.8648 (3)	0.2427 (1)	0.9068 (2)	4.06 (7)
C(11)	0.518 (1)	0.0690 (5)	0.9067 (6)	4.5 (3)
C(12)	0.445 (1)	0.0581 (5)	0.8517 (7)	6.1 (4)
C(13)	0.330 (1)	0.0650 (6)	0.8559 (7)	7.3 (4)
C(14)	0.293 (1)	0.0870 (6)	0.9181 (7)	7.2 (4)
C(15)	0.367 (1)	0.1012 (5)	0.9719 (7)	6.3 (4)
C(16)	0.482 (1)	0.0924 (5)	0.9669 (6)	5.6 (3)
C(17)	0.640 (1)	−0.0144 (5)	0.8989 (7)	7.2 (4)
C(18)	0.729 (1)	0.0648 (6)	0.9817 (6)	6.1 (4)
C(21)	0.915 (1)	−0.0363 (5)	0.8538 (6)	4.8 (3)
C(22)	0.846 (1)	−0.0772 (5)	0.8360 (7)	6.7 (4)
C(23)	0.839 (1)	−0.1189 (5)	0.8806 (7)	7.9 (4)
C(24)	0.897 (1)	−0.1167 (5)	0.9433 (8)	8.0 (4)
C(25)	0.963 (1)	−0.0784 (6)	0.9647 (7)	7.7 (4)
C(26)	0.971 (1)	−0.0352 (6)	0.9191 (7)	6.3 (4)
C(27)	1.054 (1)	0.0400 (5)	0.8121 (7)	5.8 (4)
C(28)	0.931 (1)	−0.0177 (5)	0.7090 (6)	5.5 (3)
C(31)	0.4805 (9)	0.0714 (5)	0.6206 (5)	4.6 (3)
C(32)	0.407 (1)	0.1039 (6)	0.6463 (6)	6.2 (4)
C(33)	0.301 (1)	0.0867 (7)	0.6645 (7)	8.0 (4)
C(34)	0.277 (1)	0.0368 (7)	0.6542 (7)	8.9 (5)
C(35)	0.350 (1)	0.0047 (6)	0.6294 (7)	8.2 (4)
C(36)	0.455 (1)	0.0212 (5)	0.6107 (6)	6.1 (4)
C(37)	0.689 (1)	0.0445 (4)	0.5621 (6)	5.2 (3)
C(38)	0.558 (1)	0.1249 (5)	0.5117 (6)	5.6 (4)
C(41)	0.8420 (9)	0.1607 (5)	0.4910 (5)	4.4 (3)
C(42)	0.784 (1)	0.1792 (6)	0.4311 (6)	6.4 (4)
C(43)	0.779 (1)	0.1533 (7)	0.3666 (7)	8.6 (5)
C(44)	0.836 (1)	0.1091 (6)	0.3668 (9)	9.5 (5)
C(45)	0.900 (1)	0.0879 (6)	0.4236 (8)	7.8 (4)
C(46)	0.900 (1)	0.1167 (5)	0.4875 (7)	6.9 (4)
C(47)	0.9907 (9)	0.1984 (5)	0.5958 (7)	5.6 (4)
C(48)	0.805 (1)	0.2563 (5)	0.5465 (7)	6.4 (4)
C(51)	0.4395 (9)	0.2356 (5)	0.7810 (6)	4.8 (3)
C(52)	0.385 (1)	0.2521 (7)	0.7205 (7)	7.8 (5)
C(53)	0.275 (1)	0.2401 (7)	0.7059 (8)	8.2 (5)
C(54)	0.223 (1)	0.2100 (7)	0.7512 (9)	9.2 (5)
C(55)	0.277 (1)	0.1930 (6)	0.8100 (8)	6.6 (4)
C(56)	0.387 (1)	0.2046 (5)	0.8242 (7)	5.8 (4)
C(57)	0.549 (1)	0.2873 (5)	0.8871 (7)	5.9 (3)
C(58)	0.609 (1)	0.3068 (5)	0.7500 (8)	6.4 (4)
C(61)	0.831 (1)	0.3072 (4)	0.9211 (6)	4.3 (3)
C(62)	0.847 (1)	0.3401 (5)	0.8668 (8)	7.5 (4)
C(63)	0.813 (1)	0.3914 (6)	0.876 (1)	8.9 (5)
C(64)	0.764 (2)	0.4044 (7)	0.938 (1)	12.9 (6)
C(65)	0.751 (1)	0.3715 (6)	0.9911 (9)	10.0 (5)
C(66)	0.783 (1)	0.3219 (5)	0.9841 (7)	6.1 (4)
C(67)	1.007 (1)	0.2475 (6)	0.8824 (8)	6.7 (4)
C(68)	0.887 (1)	0.2188 (5)	0.9954 (7)	7.0 (4)
C(71)	0.706 (2)	0.100 (1)	0.178 (1)	18 (1)*
C(72)	0.637 (2)	0.0768 (8)	0.210 (1)	11.4 (6)*
C(73)	0.542 (2)	0.0939 (9)	0.220 (1)	14.7 (8)*
C(74)	0.472 (2)	0.1308 (9)	0.190 (1)	13.9 (8)*
C(75)	0.539 (2)	0.159 (1)	0.150 (1)	17 (1)*
C(76)	0.652 (2)	0.1447 (9)	0.141 (1)	13.0 (7)*
C(77)	0.805 (2)	0.110 (1)	0.157 (1)	15.1 (8)*

[a] Starred values denote isotropically refined atoms. Values for anisotropically refined atoms are given in the form of the equivalent isotropic displacement parameter defined as $(4/3)[a^2\beta_{11} + b^2\beta_{22} + c^2\beta_{33} + ab(\cos\gamma)\beta_{12} + ac(\cos\beta)\beta_{13} + bc(\cos\alpha)\beta_{23}]$.

Table III. Positional and Equivalent Isotropic Displacement Parameters for $HPEt_3[Nb_3Cl_{10}(PEt_3)_3] \cdot 1.25C_7H_8$

atom	x	y	z	B,[a] Å²
Nb(1)	0.25368 (6)	0.41540 (4)	0.18335 (3)	2.83 (2)
Nb(2)	0.03433 (6)	0.35746 (4)	0.18339 (3)	2.74 (2)
Nb(3)	0.09368 (6)	0.50035 (4)	0.23471 (3)	2.86 (2)
Cl(1)	0.0830 (2)	0.4665 (1)	0.13159 (8)	3.20 (5)
Cl(2)	0.2038 (2)	0.3005 (1)	0.22032 (9)	3.34 (5)
Cl(3)	0.0224 (2)	0.3972 (1)	0.28098 (9)	3.27 (5)
Cl(4)	0.2709 (2)	0.4623 (1)	0.28044 (9)	3.44 (5)
Cl(5)	0.3462 (2)	0.5174 (1)	0.1505 (1)	4.58 (6)
Cl(6)	0.2777 (2)	0.3549 (1)	0.0954 (1)	4.40 (6)
Cl(7)	0.0271 (2)	0.2958 (1)	0.09309 (9)	4.29 (6)
Cl(8)	−0.1544 (2)	0.3875 (1)	0.1572 (1)	4.30 (6)
Cl(9)	−0.0851 (2)	0.5503 (1)	0.2111 (1)	4.56 (6)
Cl(10)	0.1639 (2)	0.6139 (1)	0.2101 (1)	4.60 (6)
P(1)	0.4513 (2)	0.3709 (1)	0.2226 (1)	4.32 (6)
P(2)	−0.0464 (2)	0.2384 (1)	0.2219 (1)	3.90 (6)
P(3)	0.0938 (2)	0.5572 (1)	0.3382 (1)	3.82 (6)
C(11)	0.5261 (9)	0.3314 (8)	0.1666 (5)	7.6 (4)
C(12)	0.5342 (9)	0.4453 (7)	0.2580 (6)	7.6 (4)
C(13)	0.468 (1)	0.2961 (7)	0.2727 (6)	7.0 (4)
C(14)	0.554 (1)	0.384 (1)	0.1223 (6)	9.2 (5)
C(15)	0.653 (1)	0.4257 (9)	0.2776 (8)	11.5 (6)
C(16)	0.432 (1)	0.3103 (8)	0.3294 (6)	9.5 (5)
C(21)	0.0439 (8)	0.1795 (5)	0.2697 (4)	4.8 (3)
C(22)	−0.0995 (9)	0.1745 (5)	0.1650 (5)	5.6 (3)
C(23)	−0.1579 (8)	0.2585 (5)	0.2629 (5)	5.2 (3)
C(24)	0.0864 (8)	0.2120 (6)	0.3277 (4)	5.2 (3)
C(25)	−0.202 (1)	0.2006 (7)	0.1252 (5)	7.5 (4)
C(26)	−0.212 (1)	0.1891 (7)	0.2837 (6)	8.2 (4)
C(31)	0.1389 (8)	0.4943 (5)	0.3979 (4)	4.7 (3)
C(32)	0.1789 (9)	0.6387 (5)	0.3544 (4)	5.2 (3)
C(33)	−0.0368 (8)	0.5920 (6)	0.3519 (5)	5.6 (3)
C(34)	0.137 (1)	0.5246 (7)	0.4595 (4)	6.6 (3)
C(35)	0.2990 (9)	0.6248 (6)	0.3618 (5)	6.4 (3)
C(36)	−0.1206 (9)	0.5322 (7)	0.3572 (6)	7.1 (4)
P(4)	0.7084 (3)	0.0375 (2)	0.4475 (2)	7.6 (1)
C(41)	0.769 (2)	−0.022 (1)	0.499 (1)	10.9 (7)*
C(42)	0.597 (1)	0.084 (1)	0.4722 (8)	7.3 (4)*
C(43)	0.818 (3)	0.105 (2)	0.438 (1)	13.8 (9)*
C(41A)	0.680 (4)	−0.022 (3)	0.501 (2)	8 (1)*
C(42A)	0.656 (5)	0.136 (3)	0.442 (3)	11 (2)*
C(43A)	0.877 (5)	0.046 (4)	0.472 (3)	12 (2)*
C(44)	0.712 (2)	−0.092 (1)	0.5043 (8)	11.9 (5)*
C(45)	0.551 (1)	0.140 (1)	0.4317 (7)	10.8 (5)*
C(46)	0.913 (2)	0.079 (1)	0.424 (1)	14.4 (7)*
C(51)	0.468 (2)	0.208 (1)	−0.0247 (9)	12.6 (6)*
C(52)	0.432 (1)	0.1684 (9)	−0.0751 (7)	10.2 (4)*
C(53)	0.323 (2)	0.156 (1)	−0.0897 (8)	11.8 (5)*
C(54)	0.245 (2)	0.174 (1)	−0.0590 (9)	12.5 (6)*
C(55)	0.290 (1)	0.2151 (9)	−0.0106 (7)	9.9 (4)*
C(56)	0.398 (1)	0.2284 (8)	0.0074 (6)	8.6 (4)*
C(57)	0.580 (2)	0.218 (1)	−0.009 (1)	15.5 (7)*
C(61)	0.463 (3)	0.4296 (7)	0.493 (2)	12 (1)*
C(62)	0.450 (4)	0.468 (2)	0.542 (2)	19 (2)*
C(63)	0.494 (4)	0.536 (2)	0.551 (1)	15 (1)*
C(64)	0.403 (4)	0.372 (3)	0.483 (2)	8 (1)*

[a] Starred values denote isotropically refined atoms. Values for anisotropically refined atoms are given in the form of the equivalent isotropic displacement parameter defined as $(4/3)[a^2\beta_{11} + b^2\beta_{22} + c^2\beta_{33} + ab(\cos\gamma)\beta_{12} + ac(\cos\beta)\beta_{13} + bc(\cos\alpha)\beta_{23}]$.

the solid-state context (i.e., fused into infinite arrays) and discrete form, we reasoned that the same might be true for the Nb_3 case. In this paper we describe syntheses of two such Nb_3 cluster species and a tantalum analogue of one of those clusters, full characterization, including X-ray crystallography, and a theoretical analysis of the bonding that provides an understanding of the dependence of the Nb–Nb bond lengths upon the number of cluster electrons available.[3]

(3) Preliminary communications of portions of this work have appeared. (a) Cotton, F. A.; Diebold, M. P.; Roth, W. J. *J. Am. Chem. Soc.* **1987**, *109*, 2833. (b) Cotton, F. A.; Kibala, P. A.; Roth, W. J. *J. Am. Chem. Soc.* **1988**, *110*, 298.

Table IV. Positional and Equivalent Isotropic Displacement Parameters for $HPEt_3[Ta_3Cl_{10}(PEt_3)_3]$

atom	x	y	z	B,[a] Å²
Ta(1)	0.41779 (5)	0.12237 (3)	0.26373 (3)	3.60 (1)
Ta(2)	0.42584 (5)	0.23251 (3)	0.36264 (3)	3.83 (1)
Ta(3)	0.21487 (5)	0.15872 (3)	0.32876 (3)	4.13 (1)
Cl(1)	0.3988 (3)	0.1167 (2)	0.3940 (2)	4.50 (8)
Cl(2)	0.4704 (3)	0.2337 (2)	0.2399 (2)	4.05 (7)
Cl(3)	0.2403 (3)	0.2744 (2)	0.3143 (2)	4.49 (8)
Cl(4)	0.2295 (3)	0.1465 (2)	0.2016 (2)	4.31 (8)
Cl(5)	0.3748 (4)	0.0084 (2)	0.2604 (2)	6.0 (1)
Cl(6)	0.6163 (3)	0.0941 (2)	0.2953 (2)	5.08 (9)
Cl(7)	0.6265 (3)	0.2197 (2)	0.4052 (2)	5.50 (9)
Cl(8)	0.3974 (4)	0.2566 (2)	0.4834 (2)	6.7 (1)
Cl(9)	0.1551 (4)	0.1747 (2)	0.4452 (2)	6.9 (1)
Cl(10)	0.1416 (4)	0.0493 (2)	0.3330 (3)	6.9 (1)
P(1)	0.4707 (3)	0.1086 (2)	0.1321 (2)	4.48 (9)
P(2)	0.4806 (4)	0.3567 (2)	0.3580 (2)	5.7 (1)
P(3)	0.0046 (3)	0.1921 (2)	0.2762 (2)	5.3 (1)
C(11)	0.607 (1)	0.1489 (9)	0.1184 (8)	6.3 (4)
C(12)	0.488 (2)	0.0235 (8)	0.1019 (9)	8.3 (5)
C(13)	0.367 (1)	0.1377 (9)	0.0574 (8)	6.8 (5)
C(14)	0.644 (1)	0.138 (1)	0.0453 (9)	7.7 (5)
C(15)	0.590 (2)	−0.012 (1)	0.140 (1)	9.4 (6)
C(16)	0.355 (2)	0.2093 (9)	0.0538 (9)	7.6 (5)
C(21)	0.548 (2)	0.3879 (9)	0.273 (2)	14.1 (9)
C(22)	0.577 (2)	0.3783 (8)	0.441 (1)	10.3 (6)
C(23)	0.368 (2)	0.417 (1)	0.347 (1)	10.3 (7)
C(24)	0.657 (3)	0.360 (2)	0.281 (2)	18 (1)*
C(25)	0.612 (2)	0.446 (1)	0.447 (1)	13.0 (8)*
C(26)	0.305 (2)	0.419 (1)	0.408 (1)	10.3 (6)*
C(31)	−0.008 (1)	0.2470 (8)	0.1980 (8)	6.1 (4)
C(32)	−0.094 (1)	0.122 (1)	0.245 (1)	10.2 (7)
C(33)	−0.078 (1)	0.232 (1)	0.3407 (9)	8.0 (5)
C(34)	−0.133 (1)	0.2691 (9)	0.1698 (9)	7.0 (5)
C(35)	−0.063 (2)	0.091 (1)	0.179 (1)	12.1 (8)
C(36)	−0.038 (2)	0.302 (1)	0.362 (1)	9.2 (6)
P(4)	0.7203 (6)	0.0601 (3)	0.4899 (3)	9.8 (2)
C(41)	0.649 (2)	0.064 (1)	0.568 (1)	10.3 (6)*
C(42)	0.745 (3)	−0.019 (2)	0.472 (2)	17 (1)*
C(43)	0.852 (3)	0.100 (2)	0.484 (2)	18 (1)*
C(44)	0.624 (2)	0.126 (1)	0.594 (2)	13.7 (9)*
C(45)	0.701 (3)	−0.048 (2)	0.412 (2)	21 (1)*
C(46)	0.925 (3)	0.099 (2)	0.547 (2)	20 (1)*

[a] Starred values denote isotropically refined atoms. Values for anisotropically refined atoms are given in the form of the equivalent isotropic displacement parameter defined as $(4/3)[a^2\beta_{11} + b^2\beta_{22} + c^2\beta_{33} + ab(\cos\gamma)\beta_{12} + ac(\cos\beta)\beta_{13} + bc(\cos\alpha)\beta_{23}]$.

Table V. Important Bond Distances (Å) in the $Nb_3Cl_7(PMe_2Ph)_6$ Molecule

Nb(1)–Nb(2)	2.825 (1)	Nb(2)–Cl(3)	2.522 (3)
Nb(1)–Nb(3)	2.831 (1)	Nb(2)–Cl(20)	2.482 (3)
Nb(2)–Nb(3)	2.836 (1)	Nb(2)–P(3)	2.693 (3)
Nb(1)–Cl(1)	2.462 (3)	Nb(2)–P(4)	2.743 (3)
Nb(1)–Cl(2)	2.530 (3)	Nb(3)–Cl(1)	2.468 (3)
Nb(1)–Cl(4)	2.478 (3)	Nb(3)–Cl(3)	2.467 (3)
Nb(1)–Cl(10)	2.496 (3)	Nb(3)–Cl(4)	2.535 (3)
Nb(1)–P(1)	2.692 (3)	Nb(3)–Cl(30)	2.472 (3)
Nb(1)–P(2)	2.724 (3)	Nb(3)–P(5)	2.699 (3)
Nb(2)–Cl(1)	2.475 (3)	Nb(3)–P(6)	2.722 (3)
Nb(2)–Cl(2)	2.478 (3)		

Experimental Section

All preparations were done under an atmosphere of argon unless stated otherwise. Standard vacuum line/Schlenk glassware techniques were used. Niobium and tantalum pentachlorides were obtained from Aesar; PEt_3 and PMe_2Ph were purchased from Strem Chemicals, Inc. $NbCl_4(THF)_2$ was prepared by the literature method.[4] Sodium amalgam was dispensed with a syringe from a stock solution, which was prepared by dissolving 0.48 or 0.96 g of sodium in 20 mL of mercury (the concentration of Na was assumed to be 1 or 2 mmol/mL of solution). ^{31}P spectra were recorded on a Varian XL-200 spectrometer.

$Nb_3Cl_7(PMe_2Ph)_6 \cdot C_7H_8$. PMe_2Ph (0.6 mL, 4 mmol) was added to a suspension of $NbCl_4(THF)_2$ (0.76 g, 2 mmol) in 20 mL of toluene, producing a red solution of the phosphine adduct. The mixture was reduced with 3.4 mmol of sodium amalgam, yielding a transient green solution, which eventually turned dark red-brown. After being stirred for 3 h, the solution was filtered and reduced in volume to about 5 mL. Addition of hexane precipitated a dark brown solid, which was washed with hexane and dried. Yield: 0.45 g, 47%. Crystals suitable for X-ray diffraction were obtained by layering the concentrated toluene solution with hexane. After this was allowed to stand for 1 to 2 days, the flask was shaken and large crystals grew within several days.

$HPEt_3[Nb_3Cl_{10}(PEt_3)_3] \cdot 1.25C_7H_8$. PEt_3 (0.6 mL, 4 mmol) was added to a suspension of $NbCl_4(THF)_2$ (0.76 g, 2 mmol) in 20 mL of toluene, yielding a light brown-red solution of $NbCl_4(PEt_3)_2$. Addition of 2 equiv of sodium amalgam followed by stirring led to a dark green solution, which eventually turned dark red. Stirring was maintained overnight. Following filtration through Celite, the solution was evaporated to a small volume (3–4 mL) and gently refluxed for 3 h. Addition of hexane precipitated a brown solid, which was filtered off and redissolved in ca. 15 mL of toluene, and the resulting solution was layered with hexane. Interdiffusion of solvents produced large dark red crystals of the complex in 30% yield.

$HPEt_3[Ta_3Cl_{10}(PEt_3)_3]$. A mixture of $TaCl_5$ (0.72 g, 2 mmol) and PEt_3 (0.6 mL, 4 mmol) in 20 mL of toluene was reduced with 4 equiv of sodium amalgam. The reaction produced a heterogeneous dark mixture of brownish coloration. As the mixture was decanted from mercury into a vial in air its color changed to clear green. The solution was stored in the open container for a few days without discoloration, and abundant precipitate was formed. The mixture was treated with THF (a roughly equal volume), and the solution was filtered to remove undissolved solid. Slow diffusion of hexane into this solution produced green crystals of the cluster (about 35%) and a small amount of white powder. The latter was readily removed by washing with hexane and decantation of the suspension.

(4) Manzer, L. *Inorg. Chem.* **1977**, *16*, 525.

Table VI. Important Bond Angles (deg) in the $Nb_3Cl_7(PMe_2Ph)_6$ Molecule

Nb(2)–Nb(1)–Nb(3)	60.19 (3)	Cl(3)–Nb(2)Cl(20)	95.6 (1)
Nb(1)–Nb(2)–Nb(3)	60.02 (3)	Cl(3)–Nb(2)–P(3)	167.4 (1)
Nb(1)–Nb(3)–Nb(2)	59.79 (3)	Cl(3)–Nb(2)–P(4)	75.04 (9)
Cl(1)–Nb(1)–Cl(2)	109.57 (9)	Cl(20)–Nb(2)–P(3)	80.3 (1)
Cl(1)–Nb(1)–Cl(4)	110.9 (1)	Cl(20)–Nb(2)–P(4)	80.9 (1)
Cl(1)–Nb(1)–Cl(10)	89.0 (1)	P(3)–Nb(2)–P(4)	92.48 (9)
Cl(1)–Nb(1)–P(1)	82.5 (1)	Cl(1)–Nb(3)–Cl(3)	110.38 (9)
Cl(1)–Nb(1)–P(2)	167.0 (1)	Cl(1)–Nb(3)–Cl(4)	108.8 (1)
Cl(2)–Nb(1)–Cl(4)	85.7 (1)	Cl(1)–Nb(3)–Cl(30)	90.6 (1)
Cl(2)–Nb(1)–Cl(10)	98.0 (1)	Cl(1)–Nb(3)–P(5)	81.7 (1)
Cl(2)–Nb(1)–P(1)	167.9 (1)	Cl(1)–Nb(3)–P(6)	169.1 (1)
Cl(2)–Nb(1)–P(2)	74.2 (1)	Cl(3)–Nb(3)–Cl(4)	88.3 (1)
Cl(4)–Nb(1)–Cl(10)	157.4 (1)	Cl(3)–Nb(3)–Cl(30)	156.1 (1)
Cl(4)–Nb(1)–P(1)	91.2 (1)	Cl(3)–Nb(3)–P(5)	92.4 (1)
Cl(4)–Nb(1)–P(2)	81.5 (1)	Cl(3)–Nb(3)–P(6)	79.6 (1)
Cl(10)–Nb(1)–P(1)	80.5 (1)	Cl(4)–Nb(3)–Cl(30)	96.0 (1)
Cl(10)–Nb(1)–P(2)	78.1 (1)	Cl(4)–Nb(3)–P(5)	168.5 (1)
P(1)–Nb(1)–P(2)	93.7 (1)	Cl(4)–Nb(3)–P(6)	75.1 (1)
Cl(1)–Nb(2)–Cl(2)	110.9 (1)	Cl(30)–Nb(3)–P(5)	78.9 (1)
Cl(1)–Nb(2)–Cl(3)	108.37 (9)	Cl(30)–Nb(3)–P(6)	78.8 (1)
Cl(1)–Nb(2)–Cl(20)	89.7 (1)	P(5)–Nb(3)–P(6)	93.7 (1)
Cl(1)–Nb(2)–P(3)	83.66 (9)	Nb(1)–Cl(1)–Nb(2)	69.80 (8)
Cl(1)–Nb(2)–P(4)	170.3 (1)	Nb(1)–Cl(1)–Nb(3)	70.10 (7)
Cl(2)–Nb(2)–Cl(3)	87.4 (1)	Nb(2)–Cl(1)–Nb(3)	70.03 (8)
Cl(2)–Nb(2)–Cl(20)	157.1 (1)	Nb(1)–Cl(2)–Nb(2)	68.66 (8)
Cl(2)–Nb(2)–P(3)	91.8 (1)	Nb(2)–Cl(3)–Nb(3)	69.26 (8)
Cl(2)–Nb(2)–P(4)	78.01 (9)	Nb(1)–Cl(4)–Nb(3)	68.77 (8)

Table VII. Important Bond Distances (Å) for $HPEt_3[M_3Cl_{10}(PEt_3)_3]$ (M = Nb, Ta)[a]

	Nb	Ta		Nb	Ta
M(1)–M(2)	2.972 (1)	2.931 (1)	M(2)–Cl(3)	2.452 (2)	2.426 (4)
M(1)–M(3)	2.969 (1)	2.938 (1)	M(2)–Cl(7)	2.419 (2)	2.423 (4)
M(2)–M(3)	2.988 (1)	2.928 (1)	M(2)–Cl(8)	2.434 (2)	2.389 (4)
M(1)–Cl(1)	2.503 (2)	2.489 (3)	M(2)–P(2)	2.668 (3)	2.651 (4)
M(1)–Cl(2)	2.440 (2)	2.440 (3)	M(3)–Cl(1)	2.505 (2)	2.511 (3)
M(1)–Cl(4)	2.439 (2)	2.431 (3)	M(3)–Cl(3)	2.456 (2)	2.429 (4)
M(1)–Cl(5)	2.427 (3)	2.408 (4)	M(3)–Cl(4)	2.440 (2)	2.430 (3)
M(1)–Cl(6)	2.427 (3)	2.422 (4)	M(3)–Cl(9)	2.429 (2)	2.410 (4)
M(1)–P(1)	2.661 (2)	2.646 (4)	M(3)–Cl(10)	2.408 (3)	2.427 (4)
M(2)–Cl(1)	2.505 (2)	2.496 (4)	M(3)–P(3)	2.671 (3)	2.650 (4)
M(2)–Cl(2)	2.431 (2)	2.432 (3)			

[a] Numbers in parentheses are estimated standard deviations in the least significant digits.

Table VIII. Important Bond Angles (deg) for $HPEt_3[Nb_3Cl_{10}(PEt_3)_3]\cdot 1.25C_7H_8$[a]

Nb(2)-Nb(1)-Nb(3)	60.38 (3)	Cl(3)-Nb(2)-Cl(7)	167.80 (8)
Nb(1)-Nb(2)-Nb(3)	59.75 (3)	Cl(3)-Nb(2)-Cl(8)	88.52 (8)
Nb(1)-Nb(3)-Nb(2)	59.86 (3)	Cl(3)-Nb(2)-P(2)	81.48 (8)
Cl(1)-Nb(1)-Cl(2)	105.27 (7)	Cl(7)-Nb(2)-Cl(8)	88.81 (8)
Cl(1)-Nb(1)-Cl(4)	105.81 (7)	Cl(7)-Nb(2)-P(2)	86.37 (8)
Cl(1)-Nb(1)-Cl(5)	87.80 (8)	Cl(8)-Nb(2)-P(2)	82.60 (8)
Cl(1)-Nb(1)-Cl(6)	88.14 (7)	Cl(1)-Nb(3)-Cl(3)	105.38 (7)
Cl(1)-Nb(1)-P(1)	169.48 (8)	Cl(1)-Nb(3)-Cl(4)	105.68 (7)
Cl(2)-Nb(1)-Cl(4)	88.35 (7)	Cl(1)-Nb(3)-Cl(9)	87.71 (8)
Cl(2)-Nb(1)-Cl(5)	166.25 (8)	Cl(1)-Nb(3)-Cl(10)	87.48 (8)
Cl(2)-Nb(1)-Cl(6)	88.16 (8)	Cl(1)-Nb(3)-P(3)	170.67 (8)
Cl(2)-Nb(1)-P(1)	82.95 (8)	Cl(3)-Nb(3)-Cl(4)	86.83 (7)
Cl(4)-Nb(1)-Cl(5)	92.20 (8)	Cl(3)-Nb(3)-Cl(9)	90.95 (8)
Cl(4)-Nb(1)-Cl(6)	166.05 (8)	Cl(3)-Nb(3)-Cl(10)	167.06 (9)
Cl(4)-Nb(1)-P(1)	80.62 (8)	Cl(3)-Nb(3)-P(3)	81.66 (8)
Cl(5)-Nb(1)-Cl(6)	88.04 (9)	Cl(4)-Nb(3)-Cl(9)	166.54 (8)
Cl(5)-Nb(1)-P(1)	83.58 (8)	Cl(4)-Nb(3)-Cl(10)	91.13 (8)
Cl(6)-Nb(1)-P(1)	85.55 (8)	Cl(4)-Nb(3)-P(3)	80.51 (7)
Cl(1)-Nb(2)-Cl(2)	105.48 (7)	Cl(9)-Nb(3)-Cl(10)	88.08 (9)
Cl(1)-Nb(2)-Cl(3)	105.48 (7)	Cl(9)-Nb(3)-P(3)	86.03 (8)
Cl(1)-Nb(2)-Cl(7)	86.39 (7)	Cl(10)-Nb(3)-P(3)	85.40 (8)
Cl(1)-Nb(2)-Cl(8)	89.37 (8)	Nb(1)-Cl(1)-Nb(2)	72.81 (6)
Cl(1)-Nb(2)-P(2)	169.29 (7)	Nb(1)-Cl(1)-Nb(3)	72.72 (5)
Cl(2)-Nb(2)-Cl(3)	88.23 (7)	Nb(2)-Cl(1)-Nb(3)	73.21 (6)
Cl(2)-Nb(2)-Cl(7)	91.32 (8)	Nb(1)-Cl(2)-Nb(2)	75.20 (6)
Cl(2)-Nb(2)-Cl(8)	165.13 (8)	Nb(2)-Cl(3)-Nb(3)	74.99 (7)
Cl(2)-Nb(2)-P(2)	82.56 (7)	Nb(1)-Cl(4)-Nb(3)	74.97 (6)

[a] Numbers in parentheses are estimated standard deviations in the least significant digits.

Table IX. Important Bond Angles (deg) for $HPEt_3[Ta_3Cl_{10}(PEt_3)_3]$[a]

Ta(2)-Ta(1)-Ta(3)	59.85 (2)	Cl(3)-Ta(2)-Cl(7)	164.8 (1)
Ta(1)-Ta(2)-Ta(3)	60.18 (2)	Cl(3)-Ta(2)-Cl(8)	92.6 (1)
Ta(1)-Ta(3)-Ta(2)	59.96 (2)	Cl(3)-Ta(2)-P(2)	81.8 (1)
Cl(1)-Ta(1)-Cl(2)	106.5 (1)	Cl(7)-Ta(2)-Cl(8)	88.0 (2)
Cl(1)-Ta(1)-Cl(4)	106.5 (1)	Cl(7)-Ta(2)-P(2)	83.3 (1)
Cl(1)-Ta(1)-Cl(5)	86.2 (1)	Cl(8)-Ta(2)-P(2)	84.0 (2)
Cl(1)-Ta(1)-Cl(6)	87.7 (1)	Cl(1)-Ta(3)-Cl(3)	106.4 (1)
Cl(1)-Ta(1)-P(1)	167.7 (1)	Cl(1)-Ta(3)-Cl(4)	105.8 (1)
Cl(2)-Ta(1)-Cl(4)	87.7 (1)	Cl(1)-Ta(3)-Cl(9)	86.9 (1)
Cl(2)-Ta(1)-Cl(5)	167.2 (1)	Cl(1)-Ta(3)-Cl(10)	87.3 (1)
Cl(2)-Ta(1)-Cl(6)	90.5 (1)	Cl(1)-Ta(3)-P(3)	170.4 (1)
Cl(2)-Ta(1)-P(1)	80.3 (1)	Cl(3)-Ta(3)-Cl(4)	88.1 (1)
Cl(4)-Ta(1)-Cl(5)	90.5 (1)	Cl(3)-Ta(3)-Cl(9)	91.3 (1)
Cl(4)-Ta(1)-Cl(6)	165.6 (1)	Cl(3)-Ta(3)-Cl(10)	166.1 (1)
Cl(4)-Ta(1)-P(1)	83.7 (1)	Cl(3)-Ta(3)-P(3)	80.0 (1)
Cl(5)-Ta(1)-Cl(6)	88.1 (1)	Cl(4)-Ta(3)-Cl(9)	166.9 (1)
Cl(5)-Ta(1)-P(1)	86.9 (1)	Cl(4)-Ta(3)-Cl(10)	90.4 (1)
Cl(6)-Ta(1)-P(1)	81.9 (1)	Cl(4)-Ta(3)-P(3)	81.2 (1)
Cl(1)-Ta(2)-Cl(2)	106.5 (1)	Cl(9)-Ta(3)-Cl(10)	87.0 (2)
Cl(1)-Ta(2)-Cl(3)	107.0 (1)	Cl(9)-Ta(3)-P(3)	85.8 (1)
Cl(1)-Ta(2)-Cl(7)	88.2 (1)	Cl(10)-Ta(3)-P(3)	86.1 (1)
Cl(1)-Ta(2)-Cl(8)	86.4 (1)	Ta(1)-Cl(1)-Ta(2)	72.0 (1)
Cl(1)-Ta(2)-P(2)	167.4 (1)	Ta(1)-Cl(1)-Ta(3)	71.96 (9)
Cl(2)-Ta(2)-Cl(3)	86.7 (1)	Ta(2)-Cl(1)-Ta(3)	71.56 (9)
Cl(2)-Ta(2)-Cl(7)	89.2 (1)	Ta(1)-Cl(2)-Ta(2)	74.0 (1)
Cl(2)-Ta(2)-Cl(8)	166.7 (1)	Ta(2)-Cl(3)-Ta(3)	74.2 (1)
Cl(2)-Ta(2)-P(2)	82.8 (1)	Ta(1)-Cl(4)-Ta(3)	74.37 (9)

[a] Numbers in parentheses are estimated standard deviations in the least significant digits.

X-ray Crystallography. General Information. Standard crystallographic procedures were used.[5] Lorentz and polarization corrections were applied. Empirical absorption correction based upon azimuthal scans was applied in the case of the Nb–PMe_2Ph and Ta–PEt_3 structures. Important crystallographic data are summarized in Table I.

In each case the use of direct methods (program MULTAN) revealed the whole M_3X_{13} unit. The remaining non-hydrogen atoms were located by series of least-squares refinements and difference Fourier syntheses. The following are additional comments pertaining to individual structure determinations.

(5) (a) Bino, A.; Cotton, F. A.; Fanwick, P. E. *Inorg. Chem.* **1979**, *18*, 3558. (b) Cotton, F. A.; Frenz, B. A.; Deganello, G.; Shaver, A. *J. Organometal. Chem.* **1973**, *50*, 227.

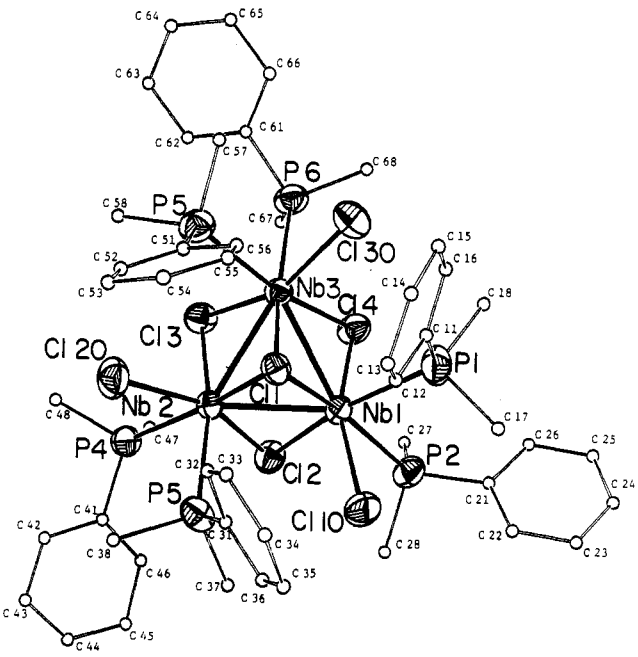

Figure 2. ORTEP drawing of the $Nb_3Cl_7(PMe_2Ph)_6$ molecule. The thermal ellipsoids are drawn at the 30% probability level. Carbon atoms have been assigned arbitrarily small thermal parameters for the sake of clarity.

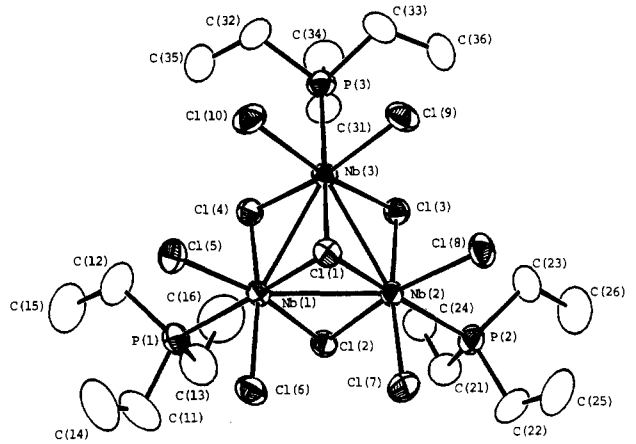

Figure 3. ORTEP drawing of the $Nb_3Cl_{10}(PEt_3)_3^-$ anion. The ellipsoids enclose 40% of electron density.

$Nb_3Cl_7(PMe_2Ph)_6\cdot C_7H_8$. All atoms in the cluster were assigned anistropic displacement parameters while the solvent molecule was refined isotropically.

$HPEt_3[Nb_3Cl_{10}(PEt_3)_3]\cdot 1.25C_7H_8$. The cation showed disorder of all three α-carbon atoms over two positions. They were assigned a fractional occupancy of 0.7 and 0.3, and each pair was connected to the same methyl group (β-carbon atom).

The crystals also contained interstitial toluene molecules, one on a general position and another around an inversion center. The latter exhibited high displacement parameters of the corresponding carbon atoms and therefore was assigned an overall site occupancy equal to 0.5. The total number of the solvent molecules in the unit cell was therefore five (four on a general position and two with a half-occupancy around inversion centers) leading to 1.25 molecules of toluene per unit formula. Since refinement of the molecule on an inversion center resulted in a distorted hexagon (C–C(Me)–C angle of 75°) a model with constraints was adopted and refined by using the program SHELX. The distances between atoms were fixed at 1.395 Å for adjacent pairs and at 2.42 Å for pairs separated by two bonds. For each symmetry-related pair, one atom had occupancy of 0.5 and the second had 0.0 occupancy, and free variables were used to impose appropriate constraints upon the positional parameters. The methyl carbon atom was refined freely.

$HPEt_3[Ta_3Cl_{10}(PEt_3)_3]$. The asymmetric cell of the Ta compound was comprised of the trinuclear anion, $Ta_3Cl_{10}(PEt_3)_3^-$, and $HPEt_3^+$ counterion. The former was refined anisotropically with the exception of three

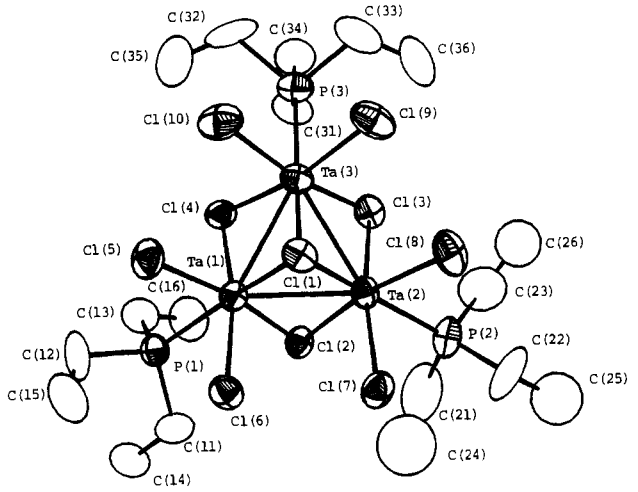

Figure 4. ORTEP drawing of the $Ta_3Cl_{10}(PEt_3)_3^-$ anion. The ellipsoids enclose 40% of electron density.

Table X. Important Averaged Interatomic Dimensions in $[M_3Cl_{10}(PEt_3)_3]^-$ (M = Nb and Ta) and $Nb_3Cl_7(PMe_2Ph)_6$

	$[M_3Cl_{10}(PEt_3)_3]^-$		
	Nb	Ta	$Nb_3Cl_7(PMe_2Ph)_6$
	Distances, Å		
M–M	2.976 [6]	2.932 [3]	2.832 [4]
$M–Cl_{cap}$	2.504 [1]	2.498 [7]	2.470 [5]
$M–Cl_{bridge}$	2.443 [4]	2.431 [3]	2.476 [3],[a] 2.531 [4][b]
$M–Cl_{terminal}$	2.424 [4]	2.413 [6]	2.485 [6]
M–P	2.667 [3]	2.649 [2]	2.696 [2],[b] 2.731 [8][c]
	Angles, deg		
$M–Cl_{cap}–M$	72.9 [2]	71.9 [1]	70.0 [1]
$M–Cl_{bridge}–M$	75.05 [7]	74.2 [2]	68.9 [2]

[a] Cl trans to $Cl_{terminal}$. [b] Cl_{bridge} and P atoms trans to each other. [c] P trans to Cl_{cap}.

terminal carbon atoms in one of the PEt_3 ligands. Only the central P atom in the cation was assigned an anisotropic displacement parameter. The final difference Fourier map contained residual electron density above 1 e $Å^{-3}$, but it was located in the proximity of the metal atoms.

Computational Procedures. Detailed description of the approximate Fenske–Hall nonempirical MO method can be found elsewhere.[6] The calculations we have done employ the idea of "clusters in molecules"[7] and begin with a calculation of the bare metal cluster, $[Nb_3]^{9+}$ or $[Nb_3]^{7+}$. Calculations for the intermediate "compounds", $[Nb_3Cl_4]^{5+}$ or $[Nb_3Cl_4]^{3+}$, which included only the capping and bridging ligands, were then performed. Finally the entire molecules were calculated, and resultant MO's were dissected into the contributions from the canonical orbitals of the bare metal clusters. In this way, the metals in the molecules are not considered individually as atoms but as cluster entities and the metal contributions to the MO's of the entire molecules were expressed in terms of the cluster MO's rather than in terms of metal atomic orbitals.

The atomic coordinates used in the calculations for the model systems, $[Nb_3Cl_{10}(PH_3)_3]^-$ and $Nb_3Cl_7(PH_3)_6$ were based on the crystal structure data of the real compounds. The molecules were idealized to have C_{3v} and C_3 symmetries, respectively. For $[Nb_3Cl_{10}(PH_3)_3]^-$, the bond distances used are Nb–Nb = 2.976 Å, $Nb–Cl_c$ (capping Cl) = 2.504 Å, $Nb–Cl_b$ (bridging Cl) = 2.443 Å, $Nb–Cl_t$ (terminal Cl) 2.424 Å, and Nb–P = 2.666 Å. For $Nb_3Cl_7(PH_3)_6$, these are Nb-Nb = 2.832 Å, $Nb–Cl_c$ = 2.470 Å, $Nb–Cl_b$ (trans to P) = 2.530 Å, $Nb–Cl_b$(trans to Cl) = 2.476 Å, Nb–P(trans to Cl_b) = 2.696 Å, and Nb–P(trans to Cl_c) = 2.731 Å. In all cases, the distance P–H has been chosen as 1.437 Å.

The atomic coordinates used in the calculations of the bare clusters and the intermediate compounds were exactly the same as those in the corresponding whole molecules. A right-hand local coordinate system for each of the metal atoms in all calculations was chosen as follows. The Z axis points toward the center of the metal triangle, the X axis is in the plane of the triangle, and the Y axis is perpendicular to the plane.

(6) Hall, M. B.; Fenske, R. F. *Inorg. Chem.* **1972**, *11*, 768.
(7) Bursten, B. E.; Cotton, F. A.; Hall, M. B.; Najjar, R. C. *Inorg. Chem.* **1982**, *21*, 302.

Table XI. Relative Energy and Atomic Orbital Contribution for Molecular Oribtals of $[Nb_3]^{9+}$

		% contribn						
		d						
orbital	energy, eV	z^2	x^2-y^2	xy	xz	yz	s	p
$1a_2'$	10.71	0	0	0	82	0	0	18
$2e''$	8.43	0	0	15	0	83	0	2
$3e'$	8.16	84	10	0	0	0	3	2
$1a_1''$	7.66	0	0	100	0	0	0	0
$2e'$	6.78	7	80	0	6	0	5	2
$1e''$	4.02	0	0	85	0	15	0	0
$2a_1'$	3.59	0	98	0	0	0	2	0
$1a_2''$	2.02	0	0	0	0	99	0	1
$1e'$	1.46	2	7	0	84	0	4	3
$1a_1'$	0.00	91	0	0	0	0	5	4

Results and Discussion

Chemistry. $Nb_3Cl_7(PMe_2Ph)_6$. This cluster was originally prepared[3a] by reducing a mixture of a Nb(III) species, viz., $Nb_2Cl_6(THT)(THF)_2$, and PMe_2Ph in THF. It was subsequently found that the trimer can be more conveniently synthesized by using $NbCl_4(THF)_2$ as the niobium-containing starting material.

The phosphorus NMR spectrum of this diamagnetic trimer in toluene contains a broad peak at −8 ppm and only at very low temperatures (−90 °C) does the expected splitting into two signals begin to emerge. This behavior is tentatively attributed to the influence of the quadrupolar moment of the ^{93}Nb nucleus, which is known[8] to cause abnormal NMR behavior of nuclei bonded to a niobium atom.

$HPEt_3[M_3Cl_{10}(PEt_3)_3]$. Previous work[9-14] on phosphine adducts of niobium and tantalum in oxidation state +3 revealed the existence of monomeric MX_3L_3 compounds and dinuclear $M_2X_6L_4$ complexes with edge-sharing bioctahedral geometry and double M–M bond. The former show a tendency toward dissociation of the neutral ligand and dimerization to form the latter complex.[10,11] Although these studies were limited mainly to PMe_3 and PMe_2Ph systems, it appeared that other phosphines would follow suit as the observed behavior was similar to that found with other transition metals. However, while the reduction of $TaCl_5 + 2PMe_3$ gave a dimeric Ta(III) complex in high yield, the analogous reaction with PEt_3 was said to give an intractable product.[9] We repeated this reaction and made similar observations: a heterogeneous mixture with an unattractive appearance and dark indefinable coloration was obtained. On the other hand, when we carried out analogous syntheses with PMe_3 or PMe_2Ph using reactants from the same batches as for PEt_3, clear dark red solutions, apparently containing well-defined complexes, were obtained. It is evident that the behavior of these systems is sensitive to the identity of the phosphine ligands.

In the $MX_3–PR_3$ systems the nuclearity of the predominant adduct is going to depend upon the phosphine/metal molar ratio. For high values, monomeric species are favored, while with ratios approaching unity, a trinuclear cluster is expected to be the major component. In our case, with 2 equiv of PEt_3/metal, there seems to exist a mixture of various $MX_3–PR_3$ species, as evidenced by the intractability of products. Trimers should be favored upon reduction in the amount of phosphine present, and the following rationalization of behavior of the Ta system can be proposed. Upon exposure to air, excess phosphine is converted to phosphine oxide, $OPEt_3$, and phosphonium ion, $HPEt_3^+$, and the equilibrium

(8) *Comprehensive Organometallic Chemistry*; Wilkinson, G., Ed.; Pergamon: New York, 1982; Vol. 3, pp 707–708.
(9) Sattelberger, A. P.; Wilson, R. B.; Huffman, J. C. *Inorg. Chem.* **1982**, *21*, 2392.
(10) Rocklage, S. M.; Turner, H. W.; Fellmann, J. D.; Schrock, R. R. *Organometallics* **1982**, *1*, 703.
(11) Luetkens, M. L.; Elcesser, W. L.; Huffman, J. C.; Sattelberger, A. P. *Inorg. Chem.* **1984**, *23*, 1718.
(12) Rocklage, S. M.; Fellmann, J. D.; Rupprecht, G. A.; Messerle, L. W.; Schrock, R. R. *J. Am. Chem. Soc.* **1981**, *103*, 1440.
(13) Green, M. L. H.; Hare, P. M. *J. Organomet. Chem.* **1987**, *330*, 61.
(14) Cotton, F. A.; Diebold, M. P.; Roth, W. J. *Inorg. Chim. Acta* **1985**, *105*, 41.

Table XII. Molecular Orbitals for $[Nb_3(\mu_3\text{-}Cl)(\mu\text{-}Cl)_3Cl_6(PH_3)_3]^-$

orbital	energy, eV	% contribn Nb	Cl_c	Cl_b	Cl_t	PH	$[Nb_3]^{9+}$ [a]
$14a_1$	−1.76	82	0	8	10	0	14% $1a_2''$, 67% $2a_1'$
18e	−4.22	81	1	0	18	0	54% 1e′, 17% 1e″, 5% 2e′
$13a_1$	−5.05	81	1	0	18	0	66% $1a_1'$, 7% $1a_2''$, 5% $2a_1'$
$6a_2$	−7.24	1	0	0	99	0	
17e	−7.53	3	1	1	93	2	
$5a_2$	−7.97	3	0	2	95	0	
16e	−8.01	3	2	0	93	2	
15e	−8.23	9	1	1	89	0	
$12a_1$	−8.37	11	0	3	84	2	3% $1a_1'$, 7% $2a_1'$
14e	−8.71	10	0	5	84	0	3% 1e′, 4% 2e′
$11a_1$	−8.74	9	0	5	85	1	4% $1a_1'$
13e	−9.22	13	0	9	78	0	3% 1e′
$10a_1$	−9.28	14	1	4	80	1	4% $1a_1'$, 6% $1a_2''$
12e	−9.42	14	0	6	79	1	3% 1e′, 4% 2e″
$4a_2$	−9.59	17	0	6	77	0	3% $1a_1''$, 13% $1a_2'$
11e	−11.43	8	1	82	6	3	5% 3e′
$9a_1$	−11.69	3	55	2	3	37	
10e	−11.92	18	15	30	6	31	5% 2e′, 6% 3e′, 5% 2e″
$8a_1$	−12.36	10	2	75	4	9	4% $2a_1'$, 4% $3a_1'$
9e	−12.37	13	57	28	2	0	5% 2e″
$3a_2$	−12.75	20	0	75	4	1	18% $1a_1''$
$7a_1$	−12.81	11	2	84	1	2	5% $2a_1'$
8e	−13.00	17	0	75	5	3	9% 1e′, 6% 1e″
$6a_1$	−13.97	24	29	11	1	35	7% $1a_1'$, 15% $1a_2''$
7e	−14.13	16	8	30	1	45	7% 1e″, 3% 2e′, 3% 2e″

[a] Contributions less than 3% are not included. Most of the MO's are also contributed by the high-lying 5s and 5p orbitals of Nb.

shifts toward a complex with low PR_3:M ratio, namely the trimer. As a result, from a heterogeneous mixture a clear green solution is obtained. It was thus a crucial factor in this process that the trinuclear Ta cluster turned out to have stability toward air. This, of course, is extremely rare for this oxidation state. The ^{31}P spectra of the mixture support this interpretation. After exposure to air, the solution was evaporated to dryness, extracted with toluene, and filtered into an NMR tube. The spectra taken at −50 °C contained three prominent sharp signals at −10.97 (PEt_3 bound to Ta), 18.45 ($HPEt_3^+$, broad doublet in H-coupled spectrum, J = 460 Hz), and 42.5 ppm ($OPEt_3$).[15]

We have noted that the Nb(III)–PEt_3 mixtures do not undergo noticeable color change upon exposure to air, but it remains to be determined how similar their behavior is to that of the Ta mixture. The formation of the trinuclear cluster anion and phosphonium cation was accomplished for niobium by heating the solution under an inert atmosphere.

Since the use of PBu_3 instead of PEt_3 has not altered the behavior of the Ta(III) complexes in terms of color changes, the reactivity and properties of the MX_3–PR_3 systems appears to be essentially the same for all the bulky phosphines. On the other hand, with PMe_2Ph, exposure to air gave only a short-lived, transient green solution, and rapid discoloration occurred.

We note here that, in some preliminary experiments by Dr. Robert Sandor of this laboratory, it has not been possible to generate discrete Nb_3 cluster species by attack of pyridine on Nb_3Cl_8. However, efforts to accomplish such a controlled degradation by ligand attack are being continued in other ways.

Crystal Structures. The atomic positional and isotropic equivalent displacement parameters for $Nb_3Cl_7(PMe_2Ph)_6$ and $HPEt_3[M_3Cl_{10}(PEt_3)_3]$, M = Nb and Ta, are presented in Tables II–IV, respectively. Important interatomic dimensions are listed in Tables V–IX. Complete listings of bond lengths and angles are included in the supplementary material. ORTEP drawings of the trinuclear clusters are shown in Figures 2–4.

In each compound the trinuclear cluster with a geometry typical for M_3X_{13} complexes is located on a general crystallographic position. For the two ionic species the location of the $HPEt_3^+$ cation suggests the presence of a Cl···H–P interaction: the P atom is 3.7–3.8 Å away from two Cl atoms, which are roughly on the side opposite the ethyl groups.

The $Nb_3Cl_7(PMe_2Ph)_6$ complex has a virtual C_3 symmetry while the two homologous M(III) compounds are C_{3v} species. Selected interatomic dimensions averaged according to these symmetries are given in Table X.

Calculations. Since the early work of Cotton and Haas,[16] the electronic structure of trinuclear complexes of transition metals has been studied extensively in terms of both SCF–Xα–SW and Fenske–Hall (FH) molecular orbital methods.[7,17-19] Cotton and co-workers also did a comparative study using the Cotton–Haas, Xα–SW, and FH methods on bonding in Re_3Cl_9,[19] and their results indicated that the description of the bonding in the molecule given by the FH and Xα–SW methods were very similar, both methods confirming the assignment of a double bond between each pair of rhenium atoms.

We now present the results of our Fenske–Hall molecular orbital calculations for two trinuclear complexes of niobium, namely $[Nb_3(\mu_3\text{-}Cl)(\mu\text{-}Cl)_3Cl_6(PH_3)_3]^-$ and $Nb_3(\mu_3\text{-}Cl)(\mu\text{-}Cl)_3Cl_3(PH_3)_6$, which serve as models for the real $[Nb_3(\mu_3\text{-}Cl)(\mu\text{-}Cl)_3Cl_6(PEt_3)_3]^-$ and $Nb_3(\mu_3\text{-}Cl)(\mu\text{-}Cl)_3Cl_3(PMe_2Ph)_6$. Both compounds contain a triangular metal cluster Nb_3 and have the same capping and bridging ligands. However, the Nb–Nb bond distances in the compounds differ considerably from one another, and the compounds differ in the number of valence electrons in the metal clusters. Thus there are six such electrons in $[Nb_3Cl_{10}(PEt_3)_3]^-$ and eight in $Nb_3Cl_7(PMe_2Ph)_6$, the later having the shorter Nb–Nb bond distance. To be consistent with the metal–metal bond distances, the two additional electrons in $Nb_3Cl_7(PMe_2Ph)_6$ would be assumed to occupy an orbital with metal–metal bonding character that is empty in $[Nb_3Cl_{10}(PEt_3)_3]^-$. One purpose of our calculations was to see if this is so, and we also wished to obtain a detailed overall description of the relevant orbitals.

Six-Electron Systems. For the metal cluster $[Nb_3]^{9+}$, the molecular orbitals obtained are listed in Table XI. The symmetry of the bare cluster is D_{3h}, and the MO's are designated accordingly. It can be seen that metal–metal interactions are predominantly distributed over the metal d orbitals, giving rise to a set of 10 MO's. The six valence electrons occupy the lowest $1a_1'$ and 1e′ orbitals. These orbitals are the bonding combinations of the $4d_{z^2}$ and $4d_{xz}$ orbitals, respectively. This results in a bond of order 1 between each pair of niobium atoms. Next to the HOMO are the $1a_2''$ and $2a_1'$ orbitals, which are both bonding combinations of the d_{yz} and $d_{x^2-y^2}$ AO's, respectively. If we compare the results in Table XI with the results for $[Mo_3]^{12+}$ in ref 7 and 20, we can see that the entire pictures of bonding in $[Nb_3]^{9+}$ and $[Mo_3]^{12+}$ are very similar. It may be noted, however, that the energy difference between the $1a_2''$ and $2a_1'$ orbitals is smaller in $[Nb_3]^{9+}$ than in $[Mo_3]^{12+}$, approximately 1.5 vs 2.2 eV. In the following we will concentrate on the calculation results for the $[Nb_3Cl_{10}(PH_3)_3]^-$ molecule. The results for $[Nb_3Cl_4]^{5+}$ will be mentioned briefly when it is necessary.

The calculated molecular orbitals for $[Nb_3Cl_{10}(PH_3)_3]^-$ are given in Table XII where the 18e and $14a_1$ orbitals are the HOMO and the LUMO, respectively. Not shown in the table are the lower lying MO's in the energy range from −13.63 to −26.87 eV, which represent essentially the chlorine 3s lone pairs and P–H bonds. The MO's in Table XII are designated according to the C_{3v} symmetry of the molecule. The last column of the table indicates percentage contributions of the $[Nb_3]^{9+}$ cluster MO's to each molecular orbital of $[Nb_3Cl_{10}(PH_3)_3]^-$.

Except for the highest three orbitals, the MO's in Table XII are essentially metal–ligand bonding orbitals or describe the 3p lone pairs of chlorine atoms. In most cases, the Nb–ligand bonding

(15) Harris, R. K.; Mann, B. E. *NMR and the Periodic Table*; Academic: New York, 1978; pp 100–103.

(16) (a) Cotton, F. A.; Haas, T. E. *Inorg. Chem.* **1964**, *3*, 10. (b) Cotton, F. A. *Ibid.* **1964**, *3*, 1217.

(17) Cotton, F. A.; Stanley, G. G. *Chem. Phys. Lett.* **1978**, *58*, 540.

(18) Bursten, B. E.; Cotton, F. A.; Green, J. C.; Seddon, E. A.; Stanley, G. G. *J. Am. Chem. Soc.* **1980**, *102*, 955.

(19) Bursten, B. E.; Cotton, F. A.; Stanley, G. G. *Isr. J. Chem.* **1980**, *19*, 132.

(20) Chisholm, M. H.; Cotton, F. A.; Fang, A.; Kober, E. A. M. *Inorg. Chem.* **1984**, *23*, 749.

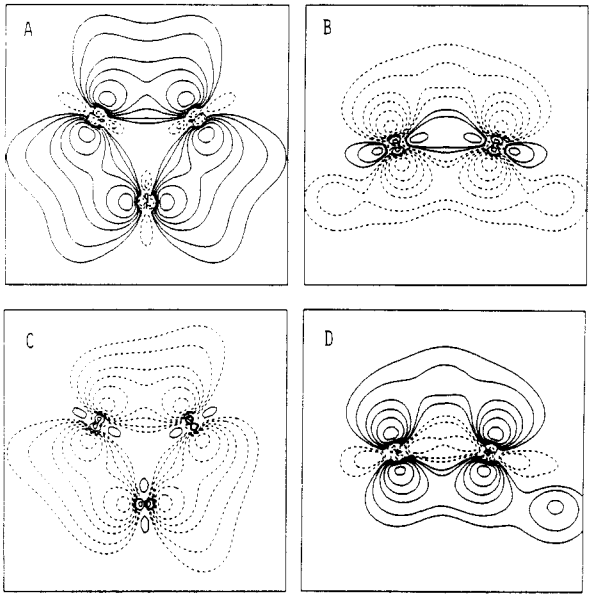

Figure 5. Contour plots of the $14a_1$ orbital of $[Nb_3Cl_{10}(PH_3)_3]^-$ (A and B) and the 20a orbital of $Nb_3Cl_7(PH_3)_6$ (C and D). A and C are plotted on the metal plane, and B and D are plotted on a plane perpendicular to the metal plane and contains one Nb–Nb bond. Positive and negative regions are represented by full and broken lines, respectively.

orbitals have mixed contributions from different types of ligands such that it is nearly impossible to give a simple description of the bonding. It is clear, however, that the metal–ligand bonds are formed basically by electron donation from the ligands to the high-lying empty MO's of $[Nb_3]^{9+}$. This is made evident by the last column of Table XII. It should be noted that upon lowering the symmetry from D_{3h} to C_{3v}, the orbital symmetries correlate as follows: a_1', $a_2'' \rightarrow a_1$; a_1'', $a_2' \rightarrow a_2$; e', $e'' \rightarrow e$. Thus, for example, the empty $1e''$, $1a_2''$, $1a_1''$, and $1a_2'$ orbitals of $[Nb_3]^{9+}$ act mainly as charge acceptors in $[Nb_3Cl_{10}(PH_3)_3]^-$ through the occupation of the 7e, $6a_1$, $3a_2$, and $4a_2$ orbitals.

Let us consider now the molecular orbitals that are most pertinent to a description of the metal–metal bonding. According to a long-established understanding of the electronic structure of compounds of this type due to Cotton,[16b] the MO's under consideration should be of a_1 and e types. As shown in Table XII, the present calculation is consistent with this prediction. The metal–metal bonding in $[Nb_3Cl_{10}(PH_3)_3]^-$ is distributed over the $13a_1$ and 18e (the HOMO) orbitals, both of which have dominant metal character. It is interesting to note the contributions of the MO's of $[Nb_3]^{9+}$ to the two Nb–Nb bonding orbitals. Due to the lowering of symmetry, both a_1'- and a_2''-type orbitals contribute to the $13a_1$ orbital, as do the e'- and e''-type orbitals to the 18e orbital. However, only the $1a_1'$ and $1e'$ orbitals make predominant contributions. Thus, the metal–metal bonding character may not change significantly from the bare cluster to the entire molecule. Therefore, we still have a single bond between each pair of niobium atoms.

The $14a_1$ orbital or the LUMO is particularly interesting; it is essentially correlated to the $2a_1'$ MO in $[Nb_3]^{9+}$. Therefore it is basically a bonding combination of the metal $4d_{x^2-y^2}$ orbitals. Actually, the $14a_1$ orbital has strong bonding character between each pair of niobium atoms. This is shown clearly by the contour plots of the orbital in Figure 5A,B.

Eight-Electron Systems. The results of the FH MO calculation on the eight-electron systems are similar to those for the six-electron systems discussed above. The MO's in Table XI can be used almost directly for the discussion of $[Nb_3]^{7+}$, except for the $1a_2''$ orbital, which is now used to accommodate two additional valence electrons. The calculated MO's for $Nb_3Cl_7(PH_3)_6$ are listed in Table XIII. By comparison of this table with Table XII, it can be seen that the MO diagram of $Nb_3Cl_7(PH_3)_6$ is very similar to that of $[Nb_3Cl_{10}(PH_3)_3]^-$. The differences in MO's come essentially from the change of some terminal ligands from one molecule to another. However, the metal–ligand bonding scheme is still much the same. Therefore, our discussion will mainly focus on the metal–metal interaction in the eight-electron systems.

Table XIII. Molecular Orbitals for $Nb_3(\mu_3\text{-Cl})(\mu\text{-Cl})_3Cl_3(PH_3)_6$

orbital	energy, eV	% contribn Nb	Cl_c	Cl_b	Cl_t	PH	$[Nb_3]^{7+}$ [a]
20a	−5.53	86	0	9	5	0	12% $1a_2''$, 72% $2a_1'$
18e	−7.71	90	1	0	8	1	64% $1e'$, 15% $1e''$, 6% $2e'$
19a	−8.29	85	1	0	14	0	71% $1a_1'$, 7% $1a_2''$, 5% $2a_1'$
17e	−10.57	4	1	3	87	5	3% $2a_1'$
18a	−10.71	4	0	3	90	3	
16e	−10.80	5	0	2	90	3	
17a	−10.83	10	0	1	85	3	7% $1a_1'$
15e	−11.73	13	0	15	70	2	4% $1e'$, 4% $2e''$
16a	−11.81	16	1	7	75	1	3% $1a_2''$, 7% $1a_2'$
14e	−12.78	10	0	66	11	13	7% $3e'$
13e	−13.25	11	0	72	3	14	4% $2e'$, 3% $3e'$, 4% $2e''$
15a	−13.47	8	1	73	2	16	
14a	−13.89	12	4	50	6	28	9% $1a_1''$
12e	−14.17	14	3	50	7	26	6% $2e''$
13a	−14.20	8	1	78	1	12	5% $2a_1'$
12a	−14.40	9	19	40	2	30	3% $1a_1''$, 3% $3a_1'$
11e	−15.07	15	35	26	1	23	5% $1e'$, 5% $1e''$
11a	−15.35	14	1	13	1	71	8% $1a_1''$
10e	−15.39	12	5	26	2	55	3% $1e'$, 4% $1e''$, 3% $2e''$
10a	−16.67	22	63	3	0	12	6% $1a_1'$, 14% $1a_2''$
9e	−16.71	15	41	9	1	34	7% $1e''$, 5% $2e'$

[a] Contributions less than 3% are not included. Most of the MO's are also contributed by the high-lying 5s and 5d orbitals of Nb.

Table XIV. Mulliken Populations of the Canonical Orbitals of $[Nb_3]^{9+}$ for $[Nb_3Cl_4]^{5+}$ and $[Nb_3Cl_{10}(PH_3)_3]^-$ and of the Canonical Orbitals of $[Nb_3]^{7+}$ for $[Nb_3Cl_4]^{3+}$ and $Nb_3Cl_7(PH_3)_6$

	six-electron systems			eight-electron systems		
MO	$[Nb_3]^{9+}$	$[Nb_3Cl_4]^{5+}$	$[Nb_3Cl_{10}(PH_3)_3]^-$	$[Nb_3]^{7+}$	$[Nb_3Cl_4]^{3+}$	$Nb_3Cl_7(PH_3)_6$
$1a_1'$	2	1.78	1.75	2	1.80	1.80
$1e'$	4	3.41	3.21	4	3.60	3.36
$1a_2''$		0.70	0.69	2	0.96	0.91
$2a_1'$		0.52	0.47		1.77	1.81
$1e''$		1.59	1.65		1.40	1.48
$2e'$		0.90	0.85		0.83	0.77
$1a_1''$		0.54	0.50		0.45	0.45
$3e'$		0.60	0.81		0.43	0.63
$2e''$		0.33	1.04		0.19	0.88
$1a_2'$		0.01	0.32		0.01	0.27

As shown in Table XIII, the Nb–Nb bonding is distributed over two a-type orbitals and one e-type orbital. Thus the 19a, 18e, and 20a MO's correlate well with the $13a_1$, 18e, and $14a_1$ orbitals in Table XII. The 20a orbital, which is now the HOMO, has dominant provenance in the $2a_1'$ MO of the bare metal cluster. Therefore it has metal–metal bonding character, just like the $14a_1$ orbital in $[Nb_3Cl_{10}(PH_3)_3]^-$. As a matter of fact, the bonding character of the 20a orbital is almost exactly the same as that of the $14a_1$ orbital, as can be seen clearly by comparing parts C and D of Figure 5 with parts A and B. Thus, we naturally expect a shorter Nb–Nb bond distance in $Nb_3Cl_7(PH_3)_6$ since the bond order between a pair of metal atoms is one-third greater than in $[Nb_3Cl_{10}(PH_3)_3]^-$.

It may be noted from Table XI that the $1a_2''$ orbital is energetically lower than the $2a_1'$ orbital. Thus, in $[Nb_3]^{7+}$, the $1a_2''$ orbital is occupied but the $2a_1'$ orbital is empty. However, our previous discussion indicates that the $1a_2''$ orbital is mainly involved in the metal–ligand bonding in the whole molecule, acting as an acceptor of charge from the ligands. This is also the case in the eight-electron system as shown in Table XIII. The situation may be understood in the following way. From Table XI we see that the $1a_2''$ orbital of the bare cluster is a linear combination of the d_{yz} AO's. Our local coordinate system on each metal is so chosen so that the orientation of the d_{yz} orbital is almost directly toward the capping ligand and a terminal ligand. As the ligands approach, it is natural that the $1a_2''$ orbital should be raised more than the $2a_1'$ orbital. Consequently, the valence electrons of the metals

originally in the $1a_2''$ orbital are transferred to the $2a_1'$ orbital where they support metal-metal bonding, and the $1a_2''$ orbital then accepts charge density from the ligands to form metal-ligand bonds.

In Table XIV we list the Mulliken populations of the canonical metal cluster orbitals for the intermediate "compounds" and for the entire molecules. It can be seen that in the six-electron systems both $1a_2''$ and $2a_1'$ orbitals accept a certain amount of charge from the ligands but the $2a_1'$ orbital is less populated. For the eight-electron systems the situation is quite different. Compared with the six-electron systems, the population in the $1a_2''$ orbital does not change significantly, even though it is fully occupied in $[Nb_3]^{7+}$. However the population in the $2a_1'$ orbital has been tremendously increased. Since the populations in other high orbitals are not greatly changed from the six-electron systems to the eight-electron systems, the $2a_1'$ orbital should owe its high charge population to the electrons originally occupying the $1a_2''$ orbital in $[Nb_3]^{7+}$.

One may also notice that the metal-metal bonding orbitals in $[Nb_3Cl_{10}(PH_3)_3]^-$ are not "purely" contributed by the niobium atoms (see Table XII). Both $13a_1$ and 18e orbitals have non-negligible contributions from the terminal chlorine ligands, so that the metal-metal bonding is "perturbed". However, the contributions of the terminal chlorine atoms to the 19a and 18e orbitals are significantly decreased in $Nb_3Cl_7(PH_3)_6$, mainly because the molecule has fewer terminal chlorine atoms. This may be an indication that in some cases the terminal ligands may influence the metal-metal bond strength or may change the bonding scheme in molecules of this type.

Concluding Remarks. It has now been demonstrated that triniobium chloro/phosphine cluster compounds closely similar to the $Nb_3Cl_4Cl_{3/3}Cl_{6/2}$ subunits in Nb_3Cl_8 can be made, as well as a similar tantalum compound (although Ta_3Cl_8 is unknown). It is interesting that the cluster electron counts for our discrete species (six, eight) bracket that for the subunit in Nb_3Cl_8 (seven). It should be noted that we do not believe that the Nb-Nb distance in Nb_3Cl_8 should be compared with those found in the discrete clusters because constraints specific to the extended array may have a strong influence on this. However, the two discrete species can reasonably be compared with each other, and the relationship between them is satisfactorily explained by the molecular orbital calculations. These calculations show that there are six M-M bonding electrons in the six-electron system and eight in the eight-electron system, whereas in earlier work it appeared that the role of the last two electrons of an eight-electron system containing molybdenum atoms might be nonbonding or even slightly antibonding.

Acknowledgment. We are grateful to the Robert A. Welch Foundation for support (Grant No. A-494).

Supplementary Material Available: Full listings of bond distances and bond angles and anisotropic displacement parameters for the crystal structures of $Nb_3Cl_7(PMe_2Ph)_6 \cdot C_7H_8$, $HPEt_3[Nb_3Cl_{10}(pEt_3)] \cdot 1.25C_7H_8$, and its Ta analogue (20 pages); tables of observed and calculated structure factors for all three structures (78 pages). Ordering information is given on any current masthead page.

Notes

Contribution from the Department of Chemistry and Biochemistry, University of California, Los Angeles, California 90024-1569

Angular-Overlap Interpretation of σ and π Bonding of PF_3 and PCl_3 in $PtCl_3L^-$ Complexes

Huey-Rong Jaw and Jeffrey I. Zink*

Received March 4, 1988

The determination of the magnitudes of σ and π interactions of trihalophosphine ligands with transition metals has attracted widespread interest. The PF_3 ligand is generally considered to be similar to CO in its properties, but direct comparison of the individual σ and π components with those of other ligands is scarce.

The most insight into the σ and π properties has been obtained from vibrational spectroscopic studies of substituted metal carbonyl compounds.[1] The common lists of π acceptor ligand series have been derived from trends in carbonyl stretching frequencies.[1,3] For the trihalophosphine ligands and comparison ligands to be treated in this paper, the σ donor trend is $P(n\text{-}Bu)_3 > PF_3 \approx PCl_3 > CO$ and the π acceptor trend is $PF_3 > CO > PCl_3 > P(n\text{-}Bu)_3$. Additional insight into the relative σ and π properties has been provided by UV-PES,[4-6] molecular orbital theoretical studies,[7,8] and mass spectroscopic studies.[9,10]

Another experimental method of determining the σ and π interactions of ligands with transition metals is electronic absorption spectroscopy. The σ and π interactions can be determined from the d-d transition energies and interpreted by using the angular-overlap theory.[11,12] A series of compounds that is proving to be amenable to detailed study is the $PtCl_3L^{n-}$ series, where L can range from "Werner" ligands[13-21] to ligands of organometallic interest such as olefins,[22,23] phosphines,[24,25] CO,[26] carbenes, and acetylenes. Only the ligand L is changed in this series. Hence, systematic changes in the σ and π properties can be interpreted from analysis of the electronic spectra.

We report here electronic spectroscopic results for $(Pr_4N)[PtCl_3PF_3]$ and $(Pr_4N)[PtCl_3PCl_3]$. The spectra are analyzed by using the angular-overlap theory, and the σ and π interaction parameters are determined. The σ and π properties of PF_3 and

(1) Graham, W. A. G. *Inorg. Chem.* **1968**, *7*, 315.
(2) (a) Cotton, F. A.; Wilkinson, G. *Advanced Inorganic Chemistry*; Wiley: New York, 1980; p 1078. (b) Huheey, J. E. *Inorganic Chemistry*; Harper and Row: New York, 1983; p 432.
(3) Timney, J. A. *Inorg. Chem.* **1979**, *18*, 2502.
(4) Yarbrough, L. W.; Hall M. B. *Inorg. Chem.* **1978**, *17*, 2269.
(5) Avanzino, S. C.; Chen, H.-W.; Donahue, C. J.; Jolly, W. L. *Inorg. Chem.* **1980**, *19*, 2201.
(6) Daamen, H.; Boxhoorn, G.; Oskam, A. *Inorg. Chim. Acta* **1978**, *28*, 263.
(7) Ziegler, T.; Rauk, A. *Inorg. Chem.* **1979**, *18*, 1755.
(8) Xiao, S.-X.; Trogler, W. C.; Ellis, D. E.; Berkovitch-Yellin, Z. *J. Am. Chem. Soc.* **1983**, *105*, 7033.
(9) Saalfeld, F. E.; Mcdowell, M. V.; Gondal, S. K.; Macdiarmid, A. G. *J. Am. Chem. Soc.* **1968**, *90*, 3684.
(10) Hitchcock, P. B.; Jacobson, B.; Pidock, A. *J. Chem. Soc., Dalton Trans.* **1977**, 2043.
(11) Schaffer, C. E.; Jørgensen, C. K. *Mol. Phys.* **1965**, *9*, 401.
(12) Schaffer, C. E. *Struct. Bonding (Berlin)* **1968**, *5*, 68.
(13) Fenske, R. F.; Martin, D. S.; Ruedenberg, K. *Inorg. Chem.* **1962**, *1*, 441.
(14) (a) Kroening, R. F.; Rush, R. M.; Martin, D. S.; Clardy, J. C. *Inorg. Chem.* **1974**, *13*, 1366. (b) Martin, D. S.; Tucker, M. A.; Kassman, A. J. *Inorg. Chem.* **1965**, *4*, 1682.
(15) Fanwick, P. E.; Martin, D. S. *Inorg. Chem.* **1973**, *12*, 24.
(16) Martin, D. S. *Inorg.* Chim. *Acta, Rev.* **1971**, *5*, 107.
(17) Patterson, H. H.; Godfrey, J. J.; Khan, S. M. *Inorg. Chem.* **1972**, *11*, 2872.
(18) Francke, E.; Moncuit, C. *Theor.* Chim. Acta **1973**, *29*, 319.
(19) Tuszynski, W.; Gliemann, G. *Z. Naturforsch., A: Phys., Phys. Chem., Kosmophys.* **1979**, *34A*, 211.
(20) Vanquickenborne, L. G.; Ceulemans, A. *Inorg. Chem.* **1981**, *20*, 796.
(21) Chang, T.-H.; Zink, J. I. *Inorg. Chem.* **1985**, *24*, 4499.
(22) Chang, T.-H.; Zink J. I. *J. Am. Chem. Soc.* **1984**, *106*, 287.
(23) Jaw, H.-R.; Chang, T.-H.; Zink, J. I *Inorg. Chem.* **1987**, *26*, 4204.
(24) Philips, J.; Zink, J. I. *Inorg. Chem.* **1986**, *25*, 103.
(25) Chang, T.-H.; Zink, J. I. *Inorg. Chem.* **1986**, *25*, 2736.
(26) Chang, T.-H.; Zink, J. I. *J. Am. Chem. Soc.* **1987**, *109*, 692.

0020-1669/88/1327-3421$01.50/0